Laser cooling of an indium atomic beam enabled by magnetic fields

B. Klöter,[1] C. Weber,[1] D. Haubrich,[1] D. Meschede,[1] and H. Metcalf[2]
[1]*Institut für Angewandte Physik der Universität Bonn, Wegelerstrasse 8, D-53115, Bonn, Germany*
[2]*Physics and Astronomy, Stony Brook University, Stony Brook, New York 11794-3800, USA*
(Received 25 October 2007; published 5 March 2008)

We demonstrate magnetic field enabled optical forces on a neutral indium atomic beam in a light field consisting of five frequencies. The role of dark magnetic ground state sublevels is studied and enables us to cool the atomic beam transversely to near the Doppler limit with laser frequencies tuned above the atomic resonance. The effect of laser cooling can be explained with transient effects in the light potential created by the standing wave light field where the atoms are optically pumped into the dark states and recycled by Larmor precession.

DOI: 10.1103/PhysRevA.77.033402 PACS number(s): 37.10.De, 37.10.Vz, 81.16.Ta

I. INTRODUCTION

Laser cooling of neutral atoms [1] is the central enabling tool for present day research in the field of atom optics. It serves to tightly control the motion of neutral atoms. With laser cooled atomic beams and gases, such diverse applications as atomic nanofabrication [2], atom interferometry, and the generation of matter waves [3] has become possible.

In contrast to its widespread use, however, the application of laser cooling remains restricted to relatively few atoms. Except for the alkalis, alkaline earths, and metastable rare gas atoms, only a few atoms offer an accessible, low-lying optical electronic transition that is both closed and strong to enable the most convenient requirement for laser cooling. Less conventional atoms for which ground-state laser cooling with cycling transitions has been realized in past years are easily counted, they include Cr [4], Fe [5], Yb [6], Ag [7], and Er [8].

Group III elements in the periodic table are interesting candidates for atomic nanofabrication since they could be used to create novel composite materials with full three-dimensional (3D) structuring during deposition [9], a unique promise of atomic nanofabrication. It has been shown that laser cooling can straightforwardly be applied to Al [10] and Ga [11] atoms by exciting their $P_{3/2} \rightarrow D_{5/2}$ cycling transition which lies in the near UV. Unfortunately, the fraction of atoms accessible in this case is limited to the thermal fraction in the $P_{3/2}$ state that typically does not exceed 10% for indium [12].

All group III atoms offer a $P_{1/2}-S_{1/2}-P_{3/2}$ electronic Λ system that involves the ground states and contains 100% of the atoms. The transition wavelengths are accessible with common laser sources. The Λ system can be exploited for laser cooling provided that a sufficiently large rate of light absorption is maintained. The main obstruction for a high absorption rate is the well known formation of (coherent) dark states in Λ systems or in integer $J \rightarrow J$ $(M=0 \rightarrow 0)$ transitions. The solution and its application to light forces on indium is presented in this paper.

II. THE FIVE FREQUENCY Λ-TYPE LASER COOLING TRANSITION

A closed Λ-type laser cooling scheme for ^{115}In ($I=9/2$, 95% natural abundance) requires at least five frequencies with wavelengths at $\lambda=410$ and 451 nm that connect the ground states to the $6^2S_{1/2}$ excited state. (see Fig. 1). The atomic ground state of Indium is 5^2P and it has two sublevels $J=1/2,3/2$. The hyperfine interaction splits the $5P_{1/2}$ state into $F=4,5$, the $6S_{1/2}$ state into $F'=4,5$, and the $5P_{3/2}$ state into $F''=3$, 4, 5, and 6, altogether making a quite complicated spectrum. We tune all laser frequencies to excite the $6^2S_{1/2}$ $F'=5$ sublevel so that there are no transitions in or out of $5P_{3/2}$ $F''=3$ which contains less than 4% of all atoms at 1200 °C.

Even if the atom interacts with a linearly polarized light field consisting of these five frequencies there are still four Zeeman sublevels that are not coupled because of the selection rules. As a result of optical pumping, atoms will be quickly trapped in these levels and no longer interact with the laser light. For an indium atom in a light field connecting the $6S_{1/2}$, $F'=5$ level with the corresponding ground states it takes on average 11 absorption events before the atom is pumped into a dark level, thus preventing efficient Doppler cooling.

This leak in the cycling transition scheme can be closed by applying an external magnetic field of a few Gauss. A field with a component perpendicular to the optical electric field that otherwise defines the z axis causes Larmor precession [14] that recouples atoms in the dark states to the light field through mixing of the Zeeman sublevels. It is important that the Zeeman shift of the atomic levels due to the magnetic field is small with respect to the natural linewidth. Otherwise less light will be absorbed as a result of the detuning.

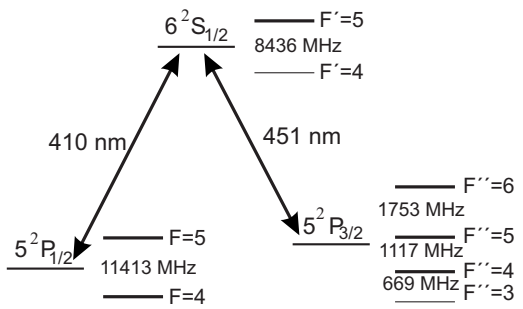

FIG. 1. Energy level scheme of ^{115}In. The lasers in the experiment address the $P_{1/2}$ $F=4,5$ to $S_{1/2}$ $F'=5$ and $P_{3/2}$ $F''=4,5,6$ to $S_{1/2}$ $F'=5$ transitions.

 ©2008 The American Physical Society

The time scale is set by the absorption rate R. For this closed six-level system with $i=5$ ground states, it can be expressed as $R=\Gamma\rho_{ee}$ where $\Gamma=2\pi\times 25.1$ MHz is the natural linewidth and ρ_{ee} is the excited state population. It can be calculated for the six states from a rate equation model as

$$\rho_{ee}=\frac{1}{6}\left(1+\sum_{i=1}^{5}\frac{\Gamma_i}{\Gamma\cdot s_i}\right)^{-1},\quad s_i=\frac{\Omega_i^2}{4\Delta_i^2+\Gamma^2},\tag{1}$$

where Γ_i is the linewidth for the ith transition. Here s_i is the corresponding saturation parameter for the transition from the ith ground state with electric dipole coupling strength defined by the Rabi frequency Ω_i, and Δ_i is the frequency detuning (all excitations are to the $6^2S_{1/2}$, $F'=5$ sublevel). This leads to effectively higher saturation intensities than calculated with a simple three level model. For example, the saturation intensity for $F''=6\rightarrow F'=5$ transition at 451 nm is 90 mW/cm^2 instead of 37 mW/cm^2. For the experimental parameters given below, R is about 1.7×10^7 s^{-1}.

III. SETUP

Two grating stabilized diode lasers provide the two frequencies at $\lambda=410$ nm. They have an output power of 14 mW to excite the $5P_{1/2}$ $F=4$ sublevel and 7 mW for the $F=5$, and they are both frequency stabilized to the atomic resonances by means of saturation spectroscopy in an all sapphire cell [13]. The two diode laser beams are combined on a polarizing beam splitter cube to make a two-frequency beam with orthogonal linear polarizations.

The $\lambda=451$ nm light is generated with a Ti:sapphire laser system. The 900 mW beam at $\lambda=902$ nm is frequency doubled in an enhancement cavity with a periodically poled KTP crystal (Raicol). The output at $\lambda=451$ nm of typically 150 mW is split into two beams with a ratio of 2:1. The beam containing the higher power is sent through a 1.435 GHz electro-optic modulator (EOM) and the other part through an acousto-optic (AOM) modulator to generate the necessary frequencies for the transitions. The two frequencies that excite the $5P_{3/2}$ states with $F''=4$ and $F''=6$ to the $6S$, $F'=5$ consist of the sidebands from the EOM. The light to excite the $5P$, $F''=5$ state is produced by the AOM. The resulting two-frequency and one-frequency beams, from the EOM and AOM, are then combined on a polarizing beam splitter cube, and similar to the $\lambda=410$ nm light, have orthogonal linear polarizations.

The blue and the violet beams $\lambda=410$ and 451 nm, are then combined with a dichroic mirror and directed to the atomic beam. The $\lambda=410$ nm light beam has an elliptical shape with waist sizes of 1 mm perpendicular to the atomic beam and 1.4 mm along the atomic beam. The 451 nm light beam has waist sizes of 1.4 mm in both directions. The Rabi frequencies are calculated to be between 0.4Γ and 1.6Γ.

The vertical atomic beam is generated *in vacuo* with a commercial effusion cell (VTS-Schwartz) which is heated to 1200 °C. The most probable longitudinal velocity is measured to be $v_l=560$ m/s. The beam is precollimated by a mechanical aperture to a divergence of 4 mrad half width at half maximum (HWHM), corresponding to a r.m.s. transverse velocity of ~ 2.4 m/s.

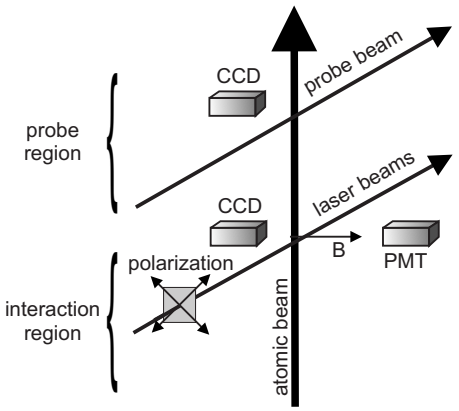

FIG. 2. Schematic of the experimental setup. The two interaction zones are 60 cm apart.

The atomic beam is crossed by light beams in two places as shown in Fig. 2. In the lower (first) one all five frequencies are present and the optical forces studied in this paper are generated there. The induced fluorescence is monitored with both a CCD camera and a photomultiplier tube (PMT). After this interaction with the laser beams, the atoms undergo free flight for $l=60$ cm to the second region. At this position is a sheet of light with only one of the $\lambda=410$ nm frequencies ($F=4\rightarrow F'=5$) present, and the fluorescence is imaged by a CCD camera to measure the spatial effect produced by the light beams in the lower region. As the intensity of this light sheet is well above the saturation limit every indium atom scatters an average of 1.3 photons, rendering the fluorescence intensity directly proportional to the atomic beam density.

A homogeneous magnetic field B is generated by two coils to be transverse to the $\vec{k}$ vectors of the light field and at 45° to their linear polarization vectors as shown in Fig. 2. The influence of residual magnetic fields of the unshielded setup is below the limit of detection (≈ 0.1 G).

For convenience, Table I lists several parameters relevant to laser cooling of ^{115}In, and some of the parameters of our setup. For wavelength dependent parameters we took the average of $\lambda=430.5$ nm.

IV. EXPERIMENT

A. Effect of applied magnetic field

In the first experiment we study the dependence of the fluorescence from the five-frequency driven indium Λ system on the external magnetic field B. All laser frequencies are tuned to resonance and the induced atomic fluorescence is detected with a PMT and a CCD camera as a function of B. At $B=0$ the spatial profile of the fluorescence along the atomic beam axis is observed to degrade in about $x\sim 1$ mm because of optical pumping into dark states. This typical length scale x is set by the time needed to pump the atoms into the dark states. It can be calculated from the absorption rate R to be $x\approx 2v_\ell n/R\approx 0.75$ mm, where $n=11$ is the average number of absorption events without magnetic field. This agrees well with the observed 1 mm.

TABLE I. Some of the parameters relevant to laser cooling of ^{115}In and some of those relevant to our experiment. Wavelength dependent parameters were calculated with the average of $\lambda = 430.5$ nm.

Property	Formula	Value
Lifetime	τ	6.3 ns
Decay rate	$\Gamma \equiv 1/\tau$	$2\pi \times 25.1$ MHz
Doppler capture velocity	$v_c \equiv \Gamma/k$	10.8 m/s
Recoil velocity	$v_r \equiv \hbar k/M$	8.0 mm/s
Velocity at Doppler limit	$v_D = \sqrt{v_r v_c/2}$	20.1 cm/s
Recoil frequency	$\omega_r \equiv \hbar k^2/2M$	$2\pi \times 9.4$ kHz
Cooling ratio	$\epsilon \equiv \omega_r/\Gamma$	3.6×10^{-4}
Cooling beam waist	$z_1/2$	1.4 mm
Free flight distance	l	60 cm
Longitudinal velocity	v_l	560 m/s
Beam divergence (HWHM)	θ	4 mrad
Interaction time	z_1/v_l	5 μs $\sim 800\tau$

However, a small transverse magnetic field produces the expected Gaussian shape of the fluorescence spot caused by the laser beam profiles with a full width at half maximum of $\sim$2.8 mm, indicating that the dark states have been depopulated. The optimal value of B is obtained by measuring the total emitted fluorescence as a function of B. This is shown in Fig. 3. Qualitatively, the signal can be understood as a competition between optical pumping into a dark state and the Larmor precession caused by the magnetic field. The optical pumping populates the dark states whereas the magnetic field mixes the Zeeman levels thereby depleting the dark states so that the atoms can absorb light again.

If the magnetic field is too small, atoms in a dark state do not evolve out of it very quickly, and when they do they are quickly pumped back into them so that the fluorescence yield is low. If the magnetic field is too high, the atoms may precess back to the dark state before optical pumping can occur (similar to the first cycle of quantum beats) and the fluorescence drops again. Also, if the Zeeman shift is too large it causes a detuning of the levels that reduces the fluorescence further. This measurement is conceptually and by its appearance very similar to zero-field level crossing experiments (Hanle effect, see, e.g., Refs. [15,16]). A detailed analysis would require a full quantum mechanical calculation involving 64 Zeeman levels which is beyond the scope of this project.

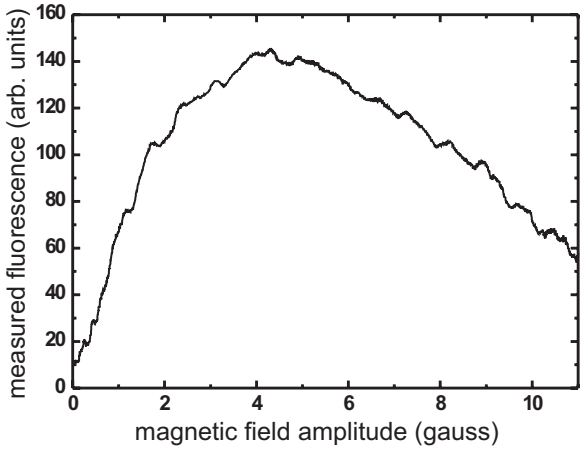

FIG. 3. Fluorescence of the atomic beam interacting with a laser beam which connects the $S_{1/2}$ $F'=5$ level with all possible ground states. A homogeneous magnetic field with varying field amplitude has been applied perpendicular to the atomic and the laser beam. The linear polarization was 45° with respect to the magnetic field.

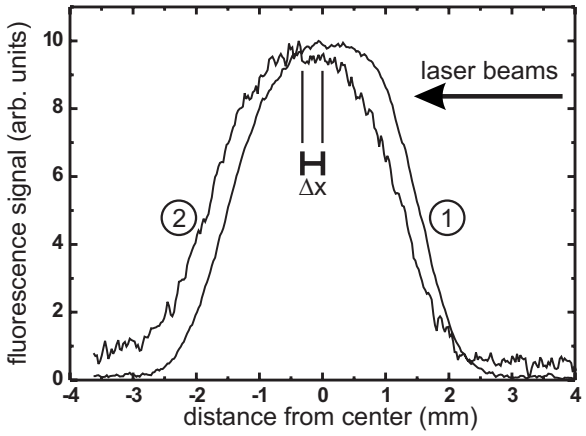

FIG. 4. Spatial distribution of the atomic beam in the probe region without (1) and with (2) applied laser beams. The lower axis gives the spatial coordinate perpendicular to the propagation axis of the atomic beam. The difference in the signal-to-noise ratio is due to optical pumping into the $P_{3/2}$ level.

Absolute calibration of the vertical axis of Fig. 3 is very difficult because of the large number of factors that determine the efficiency. These include, but are not limited to the solid angle of the detector, the transmission of the collection optics (especially off axis), imaging fidelity, and the quantum efficiency of the photocathode. A better method is the measurement of the photon momentum transfer which is described in the following section.

B. Optical deflection by the radiative force

The next step is to analyze the light forces that are exerted on the atomic beam by traveling wave laser beams (radiative force). Again the laser frequencies are tuned to resonance and the magnetic field is set to its optimum value for fluorescence of about 4 G. Figure 4 shows the spatial profile of the atomic beam in the probe region with and without applied laser beams. Its maximum transverse extent of 2.5 mm corresponds to the 4 mrad HWHM collimation of the atomic beam and its r.m.s. is about half of this. From this profile extracted from CCD picture, it is possible to determine the spatial shift Δx of the center of the atomic beam caused by the light.

From the spatial shift, the transverse velocity change Δv can be calculated using $\Delta v = v_l \Delta x/l$ where v_l and l are given in Table I. Figure 5 shows this shift as a function of total laser power, where $P_{\max}$ is the maximum laser power of each beam as given in Sec. III. The theoretical curves (solid lines)

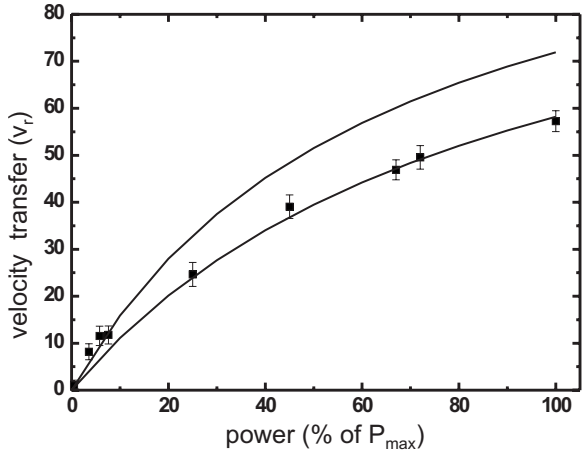

FIG. 5. Measured velocity change of the atomic beam in terms of v_r caused by laser traveling waves with all five laser frequencies tuned on resonance. The power has been changed for all beams proportionally. The polarizations were the same as used in Fig. 3 and the magnetic field strength was 4 G. The solid lines show the theoretical predictions for $\Delta=0\ \Gamma$ (upper) and $\Delta=0.35\ \Gamma$ (lower).

were determined with the rate equation model taking into account the laser beam intensity distribution along the atomic beam.

The upper curve gives the expected shift for zero detuning of the $\lambda=410$ nm and the 451 nm light and the lower one with a detuning corresponding to 0.35Γ that could arise from a deviation from perpendicularity between the laser and the atomic beam of ~ 6 mrad, and the assumptions made in the simplified rate equation model. A complementary experiment was described in Ref. [18] that used a $J=1\rightarrow J=1$ transition of metastable helium to demonstrate the role of dark states on the atomic trajectories.

From the geometry of our setup (Table I) we find that a 1 mm transverse displacement corresponds to a velocity change of 0.93 m/s=117 v_r, where $v_r \approx 8$ mm/s (Table I). Figure 4 shows that the atoms near the edge of the atomic beam, 2.5 mm from the center where $v=0$, are displaced by about the same amount as the peak. Such atoms have transverse velocities of 2.4 m/s, well within the capture velocity $\Gamma/k=10.9$ m/s. The collimating slit of $\theta \sim 4$ mrad selects velocities within the Doppler capture range only.

The maximum velocity change $\Delta v \approx 55\ v_r$ (to be compared to the r.m.s. transverse velocity of 2.4 m/s=300 v_r) is limited by finite transit time as well as by available laser power. Thus, a more sophisticated arrangement, such as that used in Ref. [17], is required to fully realize Doppler cooling by the radiative force. Nevertheless, we observed optical collimation by laser cooling with a conventional standing wave configuration of four laser beams containing five frequencies as in the deflection experiment, but arising from the dipole force. These standing waves were produced by retroreflecting the collimated laser beams.

C. Optical collimation by the dipole force

Our laser cooling experiments were implemented in one dimension by active collimation of the In atomic beam.

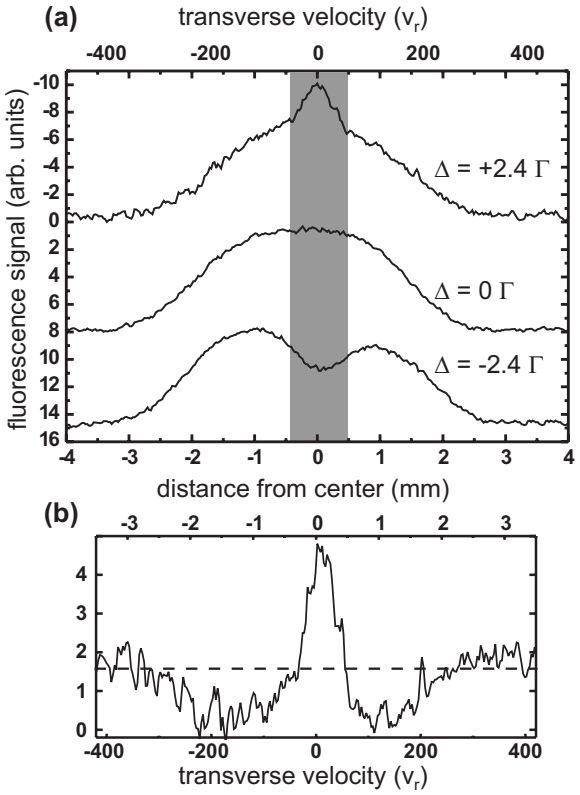

FIG. 6. Part (a) shows the spatial distribution of the atomic beam 60 cm beyond (above) a laser standing wave for both wavelengths ($\lambda=410$ nm: on resonance; $\lambda=451$ nm: $\Delta=+2.4\ \Gamma$, 0, and $-2.4\ \Gamma$ from top to bottom). All profiles have the same base line. The shaded area gives the width of the atomic beam in the standing wave zone. (b) shows the difference of the two upper curves of (a). The vertical axis is enlarged for clarity, but the horizontal scale matches that of (a).

However, we observed such collimation when the light frequency was tuned to the blue side of resonance, as shown in Fig. 6(a), in contrast to the usual laser cooling configurations (e.g., optical molasses) where the light is tuned to the red side.

Figure 6(a) shows the observed spatial distribution of the atomic beam in the probe region after interaction with standing wave beams of both wavelengths, with the $\lambda=410$ nm tuned to resonance and the $\lambda=451$ nm having three different detunings $\pm 2.4\ \Gamma$ and approximately on resonance. The probe laser was tuned to the $F=4\rightarrow F'=5$ transition, but apart from optical pumping effects, the signals were about the same when it was tuned to $F=5\rightarrow F'=5$. The region of optimal heating and cooling extends from $\pm 2\ \Gamma$ to $\pm 4\ \Gamma$. Outside of this region the efficiency quickly degrades. At small detunings of $-\Gamma/2$ there were hints of red detuned cooling, but this was not further investigated because of the poor signal to noise ratio.

The interaction time for these data was doubled by reflecting the standing waves so that the atoms traversed them twice (see below). The shaded area shows the width of the atomic beam in the standing wave zone after the mechanical collimation and therefore the ultimate width that could be achieved by collimation. There is clear evidence for cooling

on the blue side and heating on the red side of resonance, and also that for a subset of the atoms, the cooling is close to optimal. The symmetry of the profiles suggests that the laser and atomic beams are very nearly perpendicular. The polarizations of the standing waves can be chosen with $\lambda/4$ plates. We observed that the signals were the same for lin$\perp$lin, lin$\parallel$lin, and $\sigma^+\sigma^-$ polarization.

Figure 6(b) shows the difference of the two upper curves of (a), with the same horizontal scale. Atoms in the transverse velocity range below $\pm 200\ v_r$ are decelerated into the central peak with velocities well below $\pm 50\ v_r$, just about twice that of the Doppler cooling limit. However, the expected number of absorbed photons calculated with Eq. (1) is only about 20 for the experimental light intensities, detunings, and interaction time (see below). Thus the average velocity change is significantly higher than expected for radiative forces only.

The occurrence of laser cooling on the blue side of the resonance at a Rabi frequency comparable to Γ, combined with the presence of dark states, suggests a transient mechanism. Transient laser cooling arises when the atoms loose kinetic energy by climbing up the hills of the standing wave dipole potential and are then optically pumped into one of the dark states [19]. The applied magnetic field subsequently mixes the sublevels so that atoms can escape these dark states and the cooling cycle can repeat.

Thus we conclude that the cooling mechanism in this experiment arises from the dipole force and resembles Sisyphus cooling: Atoms decay into a dark state after climbing to the top of a light shift potential hill (antinode for blue detuning), and travel freely toward a node where the light shift is minimum. During this time the B field effectively rotates them back to a state sensitive to the light shift, so they can begin climbing a hill again.

Figure 6(b) suggests that this Sisyphus process is most efficient for atoms moving at $v \sim 100 v_r$ in a B field of ~ 4 G. Then the time for a 1 rad Larmor precession is $1/\omega_Z = \hbar/\mu_B g_F M_F B \sim 50$ ns for the typical average value $g_F M_F \approx 1/2$. During this time, atoms in a dark state at $100 v_r$ can travel about half the distance from peak to valley in the standing wave potential ($\lambda/4$), thereby continuing the energy exchange process. We point out that the magnetic field is required for enabling the cooling process, but is not the cause of the force.

From the energy perspective, we know that the loss of kinetic energy is proportional to the amount of scattered light and to the potential depth which is $U_0 = \hbar \Delta_i C_i s_i / [1 + (2\Delta_i/\Gamma)^2]$, where C_i is the transition strength. For the strongest transition $F''=6$, $m_F=0 \rightarrow F'=5$, $m_F=0$ the potential depth corresponds to $v \sim 20\ v_{\mathrm{rec}}$. Moreover, the capture velocity is estimated in Ref. [19] to be a couple of times the potential depth. Thus our measured change of $100\ v_r$ for atoms with velocities up to $200\ v_r$ is consistent with a dipole force, best described by an energy picture, rather than the radiative force whose velocity change is limited as shown in Fig. 5.

The width of the cooled peak is limited by the slit that collimates the atomic beam and is insensitive to laser power. Thus, we used the heating signal (red detuning) for further analysis. For these experiments, including the cooling data of

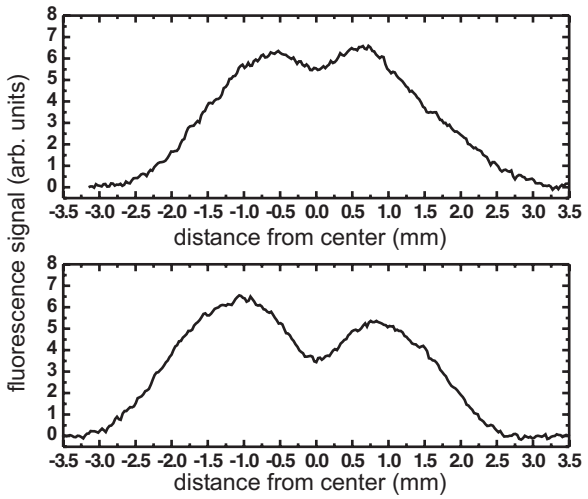

FIG. 7. Spatial distribution of the atomic beam 60 cm beyond (above) a single (top) and two (bottom) laser standing waves for both wavelengths ($\lambda=410$ nm: on resonance; $\lambda=451$ nm: $\Delta=-2.4\Gamma$).

Fig. 6, the interaction time was increased by folding the standing wave back using a retroreflecting 90° prism. Figure 7 shows the action of red-detuned light forces (heating) for a single and two spatially separated standing waves containing all wavelengths displaying the influence of the increased effective interaction time.

For the heating measurements shown in the inset of Fig. 8, atoms in the velocity range $\pm 100\ v_r$ are accelerated to higher velocities, into the vicinity of $\sim \pm 200\ v_r$ and can hence be found outside of the central dip from where they came. [The inset shows the difference between the measured velocity distributions of the unperturbed beam and the beam subject to red-detuned light similar to Fig. 6(b). The transverse velocities again correspond to 117 v_r per mm of displacement.] The data points of Fig. 8 show that the measured width as a function of the applied laser intensity, which was

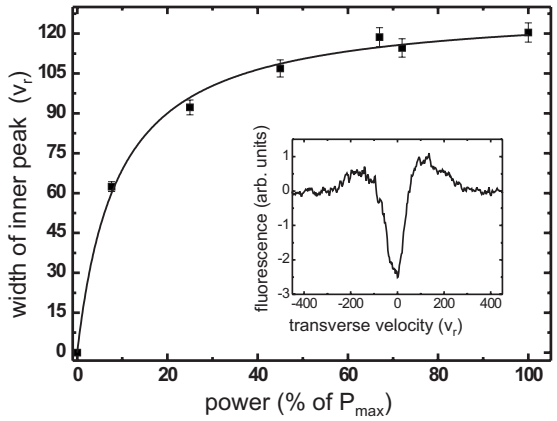

FIG. 8. The inset shows the difference between the unperturbed beam and the heated beam. A difference of two Gaussians has been fitted to the signal and the width of the inner one is plotted for different laser powers. The power has been changed for all beams proportionally. The line is proportional to the number of scattered photons.

varied with neutral density filters, saturates at about $\pm 120\ v_r$.

The solid theoretical curve in Fig. 8 is proportional to the number of absorbed photons calculated with the help of Eq. (1). Since each Sisyphus cycle requires a spontaneous emission event, this is a measure of the number of such events and hence of the total change of kinetic energy. At sufficiently high intensity, the spontaneous emission rate saturates, and there is a corresponding saturation of the width of this central dip. Thus its width is not limited by either the capture range of the radiative force $v_c=\Gamma/k$ nor by the potential depth U_0 of the dipole force, but instead by the interaction time with the laser beams.

The number of atoms within the capture velocity range v_c is given by $N(v_c)=\int_0^{v_c} f(v)dv$, where $f(v)$ is the 1D Maxwell-Boltzmann distribution. The experimental values for the fraction of heated atoms can be determined by the area of the fitted Gaussians and is plotted in Fig. 9. The curve in Fig. 9 is proportional to $N(v_c)$ where v_c is the width of the inner dip in Fig. 8.

This simple model is based on intensity gradients only and cannot explain the observed insensitivity of the cooling results to polarization gradients. As discussed in Sec. IV A, further exploration of this somewhat surprising observation would require a solution of the full system involving 64 quantum states which is beyond the scope of this article.

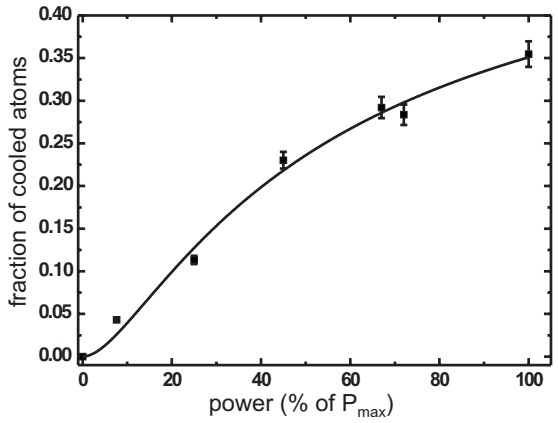

FIG. 9. Fraction of the laser heated atoms of Fig. 8 plotted for different laser powers. The power has been changed for all beams proportionally. The line is proportional to the number of addressable atoms within a capture range given by Fig. 8.

V. CONCLUSION

With an elaborate five frequency laser system we have demonstrated light pressure forces onto an In atomic beam with its complex Λ system of energy levels. We have demonstrated that the quenching of laser cooling by dark levels can be eliminated with a small magnetic field. The efficiency of laser Doppler cooling in the present setup is limited by transit times and available laser power but can be overcome with more elaborate light field schemes.

We have furthermore observed an efficient laser cooling channel for blue detuned laser frequencies resembling Sisyphus laser cooling, though with a small capture range. Theoretical estimates have shown that this effect can be explained with transient laser cooling.

ACKNOWLEDGMENTS

We wish to thank the Deutsche Forschungsgemeinschaft, and the European Commission for continued support. H.M. acknowledges the ONR and Alexander von Humbolt Stiftung. Furthermore, we are indebted to contributions by U. Rasbach, J. Wang, and R. dela Torre.

[1] H. Metcalf and P. van der Straten, *Laser Cooling and Trapping* (Springer Verlag, New York, 1999).
[2] D. Meschede and H. Metcalf, J. Phys. D **36**, R17 (2003).
[3] *Atom Interferometry*, edited by P. R. Berman (Academic, New York, 1997).
[4] R. E. Scholten, R. Gupta, J. J. McClelland, R. J. Celotta, M. S. Levenson, and M. G. Vangel, Phys. Rev. A **55**, 1331 (1997).
[5] B. Smeets, R. W. Herfst, L. P. Maguire, E. te Sligte, P. van der Straten, H. C. W. Beijerinck, and K. A. H. van Leeuwen, Appl. Phys. B: Lasers Opt. **80**, 833 (2005).
[6] M. Watanabe, R. Ohmukai, U. Tanaka, K. Hayasaka, H. Imajo, and S. Urabe, J. Opt. Soc. Am. B **13**, 2377 (1996).
[7] G. Uhlenberg, J. Dirscherl, and H. Walther, Phys. Rev. A **62**, 063404 (2000).
[8] J. J. McClelland and J. L. Hanssen, Phys. Rev. Lett. **96**, 143005 (2006).
[9] Th. Schulze, T. Müther, D. Jürgens, B. Brezger, M. K. Oberthaler, T. Pfau, and J. Mlynek, Appl. Phys. Lett. **78**, 1781 (2001).
[10] R. W. McGowan, D. M. Giltner, and S. A. Lee, Opt. Lett. **20**, 2535 (1995).
[11] S. J. Rehse, K. M. Bockel, and S. A. Lee, Phys. Rev. A **69**, 063404 (2004).
[12] S. J. Rehse, R. W. McGowan, and S. A. Lee, Appl. Phys. B: Lasers Opt. **70**, 657 (2000).
[13] U. Rasbach, J. Wang, R. dela Torre, V. Leung, B. Klöter, D. Meschede, T. Varzhapetyan, and D. Sarkisyan, Phys. Rev. A **70**, 033810 (2004).
[14] S. Slijkhuis, G. Nienhuis, and R. Morgenstern, Phys. Rev. A **33**, 3977 (1986).
[15] *Progress in Atomic Spectroscopy*, edited by W. Hanle and H. Kleinpoppen (Plenum Press, New York, 1978).
[16] *Laser Spectroscopy of Atoms and Molecules*, edited by H. Walther (Springer-Verlag, Berlin, 1976).
[17] M. D. Hoogerland, J. P. J. Driessen, E. J. D. Vredenbregt, H. J. L. Megens, M. P. Schuwer, H. C. W. Beijerinck, and K. A. H. van Leeuwen, Appl. Phys. B: Lasers Opt. **62**, 323 (1996).
[18] R. Kaiser, N. Vansteekiste, A. Aspect, E. Arimondo, and C. Cohen-Tannoudji, Z. Phys. D **18**, 17 (1991).
[19] S. Padua, C. Xie, R. Gupta, H. Batelaan, T. Bergeman, and H. Metcalf, Phys. Rev. Lett. **70**, 3217 (1993).